Temperature Measurements of Shock Compressed Liquid Deuterium up to 230 GPa

G. W. Collins, P. M. Celliers, L. B. Da Silva, R. Cauble, D. M. Gold, M. E. Foord, N. C. Holmes, B. A. Hammel, and R. J. Wallace
Lawrence Livermore National Laboratory, Livermore, California 94551

A. Ng
University of British Columbia, Vancouver B.C., Canada
(Received 25 January 2001; published 27 September 2001)

Pyrometric measurements of single-shock-compressed liquid deuterium reveal that shock front temperatures T increase from 0.47 to 4.4 eV as the pressure P increases from 31 to 230 GPa. Where deuterium becomes both conducting and highly compressible, $30 \leq P \leq 50$ GPa, T is lower than most models predict and $T \ll T_{\text{Fermi}}$, proving that deuterium is a degenerate Fermi-liquid metal. At $P >$ 50 Gpa, where the optical reflectivity is saturated, there is an increase in the rate that T increases with P.

DOI: 10.1103/PhysRevLett.87.165504 PACS numbers: 62.50.+p, 64.30.+t, 64.70.−p

Thermodynamic properties of dense fluid hydrogen near 100 GPa are required for understanding the structure of many astrophysical objects including the Jovian planets, extrasolar giant planets, brown dwarfs, and low mass stars [1]. These same properties are also critical for demonstrating inertially confined fusion in the laboratory [2]. One exceptionally difficult region to address theoretically is where hydrogen transforms from a molecular insulator to a liquid metal [3]. Some models predict that, near 10 000 K and 100 GPa, this transformation occurs through a first order phase transition [4,5], while others predict or presume a continuous transformation [6–9]. In the vicinity of this transition, hydrogen is strongly correlated, partially degenerate composite of H_2, H, H^+, electrons, and likely other components such as H_3, etc., where no simple approximation is available. To compound this theoretical complexity, until recently no experimental equation of state (EOS) data in the multimegabar region were available to guide predictions.

In recent experiments, we determined the pressure and density of deuterium along the principal Hugoniot up to pressures of 300 GPa [10]. The principal Hugoniot is a well-defined locus of states, each attainable by a single shock with a different pressure and starting from the same initial state [11]. Just above ~25 GPa, the shock compressibility increases dramatically and peak compressions of 6 are reached near 100 GPa. Simultaneous with the onset of high compressibility, we observe an increase in the optical reflectance at wavelengths across the visible and near infrared spectrum. At pressures above 50 GPa, the metal-like reflectance saturates at 40% and 60% for $\lambda = 404$ and 1064 nm, respectively [12]. These results confirm model predictions that connect the high compressibility along the Hugoniot to the molecular insulator to atomic metal transformation [4–6].

Temperature, T, is fundamental to thermodynamics and an important constraint to EOS models, but T is not part of the Rankine-Hugoniot relations [11] typically used to determine the pressure (P), density (ρ), and internal energy of a shock compressed state [11,13]. T must be measured separately from shock P and ρ. In this paper, we report T measurements along the principal Hugoniot up to $P = 230$ GPa. At the lowest shock pressures, temperatures agree with light gas gun data [14]. At shock pressures between 30 and 50 GPa, T is lower than many models predict. This is the same pressure range where deuterium becomes both highly compressible and reflective to optical and near infrared light. Near 50 GPa, T is more than an order of magnitude lower than the Fermi temperature, revealing that the transition to a highly reflective state is characteristic of a liquid metal and not a high temperature plasma. At $P >$ 50 Gpa, where the optical reflectivity saturates, there is an increase in the rate that T increases with P. Finally, at the highest pressures measured, the data and models are converging.

The details of the target design, experimental layout, and beam smoothing are similar to previously published Hugoniot experiments [10]. One smoothed beam of the Nova laser ($\lambda_L = 527$ nm) [15] was focused onto the target at normal incidence, driving a shock wave through the pusher and into the D_2. The laser footprint outside diameter (OD) at the target plane was between 600 μm and 1 mm, depending on focusing and phase plates [16]. Liquid D_2 was contained in a ~1.5-mm-diameter, 0.45-mm-long cylindrical hole machined into a copper block. One end of the cell was sealed with an Al or Be disk that served as a shock pusher; the opposite end of the cell was sealed with a sapphire window through which the shock emission was observed. Two x-ray-transparent Be foils glued over 0.5-mm-diameter holes drilled into the sides of the cell permitted transverse radiographic measurements of shock propagation and compression.

Pyrometric data were collected with two different experimental techniques. The absolute spectral radiance, $I(\lambda)$, of the shock front at several wavelengths was measured using a fiber-coupled multichannel pyrometer. We extracted T by fitting $I(\lambda)$ to a gray body Planck spectrum,

$$I(\lambda) = \varepsilon(\lambda)\frac{2\pi hc^2}{\lambda^5}\left(\exp\frac{hc}{\lambda k_b T} - 1\right)^{-1} \quad (1)$$

with T as a fit parameter, c, h, and k_b taking on their usual definitions, and the emissivity, $\varepsilon(\lambda)$, estimated from recent multiwavelength reflectivity data [12]. The pyrometer is similar to that described by Holmes *et al.* [14]; however, in that work ε was a wavelength independent fit parameter.

To obtain these data, light emitted from the shock front was collected and image relayed at unit magnification with two triplet achromats onto a fiber bundle composed of 10 UV-grade fibers, each 50 μm OD. The achromats were designed to have less than 1% variation in focal position over a 900–250-nm bandpass. The outer eight fibers were equally spaced around a 200-μm-diameter circle and were used to estimate shock front planarity. The two central fibers were further split tenfold, of which one path was coupled to a light source to illuminate the pusher for target alignment and to ensure that the cell filled with liquid. The remaining channels were coupled either to a photomultiplier tube with 650-ps rise time or a microchannel plate photomultiplier with approximately 200-ps rise time and filtered with a 25- or 40-nm bandpass. Calibrated neutral density filters kept the detectors within their linear range. The detector outputs were recorded on 1-GHz-bandwidth (300-ps rise time) digital oscilloscopes. The spectral radiance of the deuterium shock front was calibrated against a 2800-K tungsten lamp with a bolometric calibration traceable to the National Institute of Standards and Technology. Wavelengths used were 800, 700, 600, 500, 400, and 334 nm.

The emissivity is related to the reflectivity of a specular surface (the shock front) through $\varepsilon(\lambda) = 1 - R(\lambda)$. This, combined with recent reflectivity data for shock compressed deuterium [12], allows us to estimate $\varepsilon(\lambda)$ for all shock pressures reported in this paper. At wavelengths where $R(\lambda)$ is not explicitly measured, a Drude model fit to the $R(\lambda)$ data is used to interpolate between measured values. The wavelength dependent Drude model for the complex refractive index of a metal in the free-electron approximation is given by, $\hat{n}_s^2 = 1 - \frac{\omega_p^2}{(2\pi c/\lambda)^2}(1 + i\lambda/2\pi c\tau_e)^{-1}$, where $\omega_p = (4\pi n_e e^2/m_e)^{1/2}$ is the plasma frequency, λ is the optical wavelength, τ_e is the electron relaxation time, n_e is the carrier density, e is the electron charge, and m_e is the electron mass. From $\hat{n}_s$ we obtain $R(\lambda)$ through Fresnel's formula, $R(\lambda) = |(\hat{n}_s - n_0)/(\hat{n}_s + n_0)|^2$, where n_0 is the refractive index in the undisturbed liquid. Both n_e and τ_e are necessary to obtain $R(\lambda)$. We estimate $\tau_e = R_0/\nu_f$ which is appropriate for strongly scattering disordered systems in which the carrier mean-free path is limited to the interatomic distance, R_0, and υ_f is the Fermi velocity [17]. From τ_e and measurements of $R(1064)$, $R(400)$, and $R(800$ nm), we approximate n_e and ultimately $\varepsilon(\lambda, P)$.

T uncertainties listed for this technique are the 95% confidence interval of the nonlinear least squares fit to the data. Using transverse radiography, shock P and ρ were determined from shock speed, U_s, and particle speed, U_p, measurements made simultaneously with pyrometric measurement [10,18].

An example of intensity versus time data at several wavelengths for deuterium shocked to 91 GPa and 1 g cm^{-3} is shown in Fig. 1. At time = 0, the emission intensity increases from an instrument-limited rise time to a steady state value as the shock breaks out of the Al pusher and forms a steady shock in the deuterium. The emission intensity, and thus shock P, is roughly constant from 0 to 6 ns, and then decreases due to a reduction in shock T and P caused by a rarefaction wave catching up to the shock front. This rarefaction wave results from the termination of the laser pulse. The averaged spectral radiance between 0 and 6 ns for the calibrated wavelengths is plotted in Fig. 1(b) along with the fit to Eq. (1), resulting in $T = 1.4$ eV.

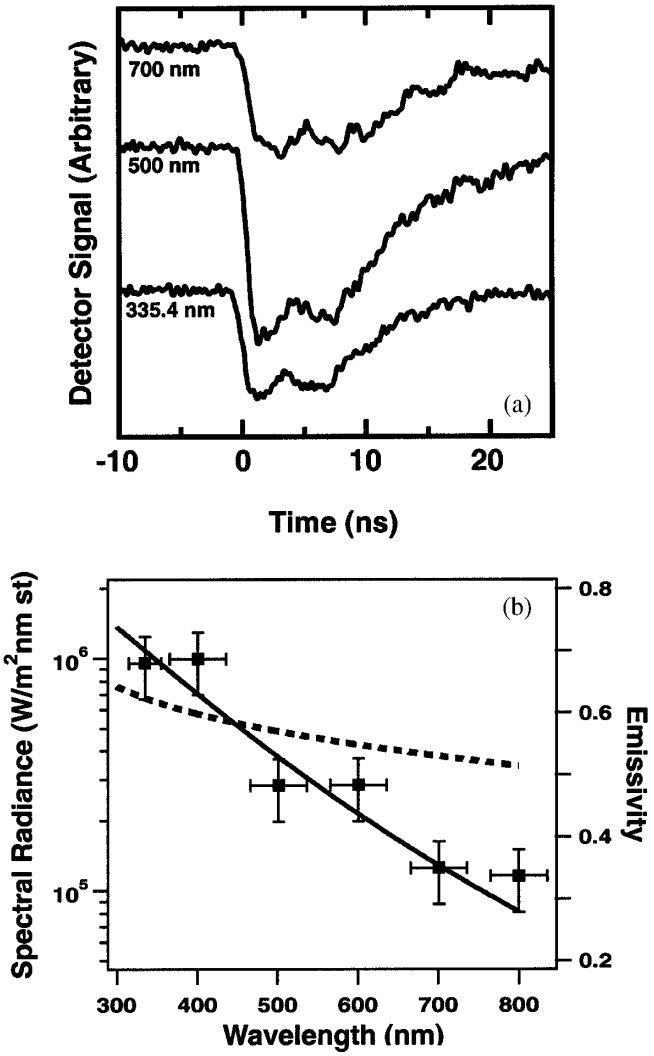

FIG. 1. (a) Detector signal versus time for several different wavelengths from D_2 shocked to 91 GPa. (b) Spectral radiance (dark squares) for the same experiment in (a) along with emissivity as described in the text (dashed line) and a gray body fit (solid line) using Eq. (1), yielding $T = 1.4$ eV. Error bars in the wavelength dimension reflect filter bandpass.

In a separate series of experiments, the spectral radiance in a single spectral band centered at 400 nm, $I(\lambda = 400\ \text{nm})$, was obtained with ~5-$\mu$m space and 20-ps time resolution. This signal was obtained by imaging the shock luminescence onto a streak camera slit. Figure 2 shows the streaked emission signal and a line out from the central part of the shock from deuterium with a shock speed $U_s = 23.4\ \mu\text{m/ns}$, corresponding to $P = 75$ GPa. The emission rise time is $t_r = 290$ ps. In general, t_r increased with increasing shock pressure above 100 Gpa, unlike the response time of the reflectivity signal [8] which was more rapid and roughly constant (<100 ps). However, the temperatures reported here are steady state values. The emission signal in Fig. 2 shows the shock is steady for more than 4 ns, after which the rarefaction from the end of the laser pulse arrives at the shock front. The absolute 400-nm emission intensity was determined by (i) measuring the optical train efficiency at 400 nm and (ii) measuring the efficiency of the streak camera with a calibrated intensity of a ~4-ns laser pulse at 532 nm and correcting for the wavelength dependence of the S-20 photocathode. Simultaneous with $I(\lambda = 400\ \text{nm})$, we recorded the shock front reflectivity at 1064-nm wavelength, $R(1064)$, and U_s, inferred from the Doppler shift of the 1064-nm probe [12]. To determine T, from $I(\lambda = 400\ \text{nm})$, we used Eq. (1) with the emissivity determined as described above. The error shown for these T values is determined by propagating uncertainties and represents the one sigma value.

Figures 3(a) and 3(b) show our experimental D_2 single shock Hugoniot T versus P (ρ), along with several model predictions. The density values in Fig. 3(b) are from Ref. [10]. Each datum is the result of a steady single shock T experiment. The inset plot of Fig. 3(a) shows $\varepsilon(\lambda)$ at $\lambda = 400$, 800, and 1064 nm versus P used for these data. Measured temperatures range from 0.47 eV at 31 GPa to 4.4 eV at 230 GPa. Temperatures are thermally equilibrated due to the more than 100 collisions that occur during the transit period of the shock through an optical skin depth.

Furthermore, even at the highest shock pressures the emission intensity is unmasked by ionization ahead of the shock front [19,20]. Between $30 < P$ (GPa) < 50, we find T is lower than predicted by most EOS models

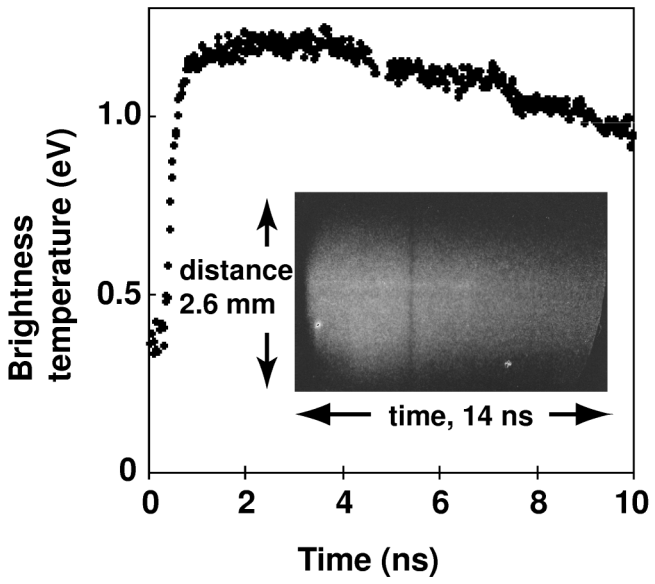

FIG. 2. The brightness temperature at 400 nm versus time, determined from the central region of the streaked shock emission data shown in the inset image. The bright spot in the image, just after shock breakout of the pusher, is a timing fiducial and the dark stripe across the image from top to bottom is caused by a defect in the output phosphor of the streak camera.

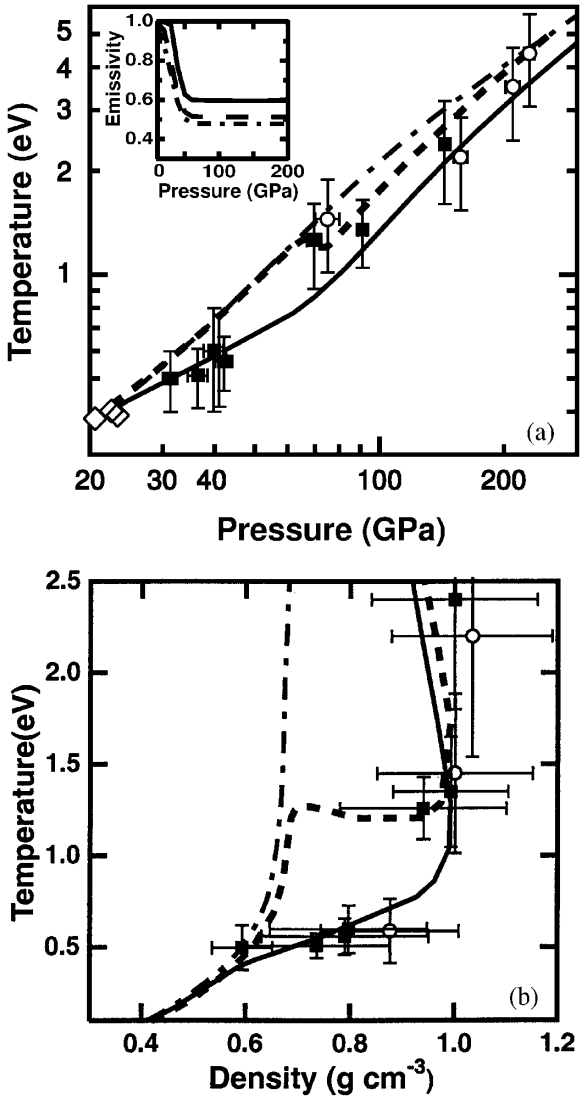

FIG. 3. (a) Temperature versus pressure for multichannel pyrometer data (solid squares) and the single wavelength streaked image data (open circles). Also shown are gas gun data [14] (open diamonds); Sesame EOS model [7] (dot-dashed line); Saumon and Chabrier EOS model [4] (dashed line), and linear-mixing EOS model [6] (solid line). The inset of (a) shows the pressure and wavelength dependent emissivity used for these data as described in the text for $\lambda = 400$ nm (dash-dotted line), $\lambda = 800$ nm (dashed line), and $\lambda = 1064$ nm (solid line). (b) Temperature versus density with same symbols as in (a).

[4,7–9]. This is the same pressure region where deuterium becomes highly compressible, as shown in Fig. 3(b) [10], and where it transitions from insulator to conductor [12]. Between 50 and 70 GPa, there is a prominent change in dT/dP. Over this pressure range the optical and near infrared reflectance saturates. Above ~70 GPa the T increases more rapidly with increasing pressure. Two of the chemical models shown in Fig. 3 predicted the large compressibility observed in laser shock experiments and connected the onset of high compressibility with the metal-insulator transition [4,6]. Neither of these models match the temperature data as well as the P-ρ data. Ross' linear-mixing model matches the data best at pressures below 50 GPa, while Saumon and Chabrier's model matches the data better at higher pressures.

The high pressures and modest temperatures reached in these experiments are in a regime where theories are immensely complicated. Near the metallization transition the average distance between electrons (or deuterons) is $1\ \text{Å} \sim 9.9 \times 10^{11}\ \text{m} = 1.87$ Bohr radii. This distance is about twice that expected for the crudest estimates for pressure induced ionization [4]. The Coulomb coupling coefficient $\Gamma = e^2/\text{Å}kT \sim 20$, so that nonideal Coulomb effects play an important role in the theory. Finally, the distance between deuterons is roughly 7.5 times their deBroglie wavelength so the deuterons behave mostly classically.

All of our measured temperatures are well below the Fermi temperature, $T_F = [\hbar^2(3\pi^2)^{2/3}/2m_e k_b]n_e^{2/3}$. For a fully ionized fluid at $1\ \text{g cm}^{-3}$ (e.g., above 100 GPa on the Hugoniot), $T_F \sim 16$ eV. This is compared to the measured temperature on the Hugoniot at ~100 GPa (near the maximum compression), where $kT \sim 1.4$ eV, or at the metallization transition [12], where $kT \sim 0.7$ eV. Since $T/T_F \ll 1$, the conducting phase produced under single shock compression is a Fermi-degenerate liquid metal, and not an ionized Maxwellian plasma. Single shock temperatures at the metallization transition are also significantly lower than previously determined estimates [21] of the band gap energy, $E_g \sim 6$–9 eV, in the semiconducting molecular fluid phase. The reverberating-shock dc conductivity measurements used to determine E_g reached densities spanning our single shock densities, but at much lower temperatures. The fact that $kT \ll E_g$ at the single shock metallization transition suggests that single shock metallization does not occur through the band gap closure of the molecular fluid proposed for reverberating-shock data.

We thank D. Saumon, M. Ross, and W. Nellis for many useful discussions. We also thank the technical staff of Nova and the cryogenics group for their exceptional effort during these experiments. Work performed under the auspices of the U.S. Department of Energy by the Lawrence Livermore National Laboratory under Contract No. W-7405-ENG-48.

[1] R. Smoluchowski, Nature **215**, 691 (1967); W. B. Hubbard, Science **214**, 145 (1981); W. B. Hubbard *et al.,* Phys. Plasmas **4**, 2011 (1997); G. Chabrier, D. Saumon, W. B. Hubbard, and J. I. Lunine, Astrophys. J. **391**, 817 (1992); D. Saumon, G. Chabrier, and H. M. Van Horn, Astrophys. J. Suppl. Ser. **99**, 713 (1995); G. Chabrier and I. Baraffe, Astron. Astrophys. **327**, 1039 (1997).

[2] S. W. Haan *et al.,* Phys. Plasmas **2**, 2480 (1995); W. J. Krauser *et al.,* Phys. Plasmas **3**, 2084 (1996); J. D. Lindl, Phys. Plasmas **2**, 3933 (1995).

[3] N. W. Ashcroft, Phys. World **8**, 43 (1995); R. J. Hemley and N. W. Ashcroft, Phys. Today **51**, No. 8, 26 (1998).

[4] D. Saumon and G. Chabrier, Phys. Rev. Lett. **62**, 2397 (1989).

[5] W. R. Magro, D. M. Ceperley, C. Pierleoni, and B. Bernu, Phys. Rev. Lett. **76**, 1240 (1996); B. Militzer, W. R. Magro, and D. M. Ceperley, in *Strongly Coupled Coulomb Systems,* edited by G. J. Kalman, K. B. Blagoev, and J. M. Rommel (Plenum Press, New York, 1998).

[6] M. Ross, Phys. Rev. B **58**, 669 (1998).

[7] G. I. Kerley, Los Alamos Laboratory Report No. LA-4776, 1972 (unpublished); G. Kerley, J. Chem. Phys. **73**, 460 (1980).

[8] M. Ross, F. H. Ree, and D. A. Young, J. Chem. Phys. **79**, 1487 (1983).

[9] T. J. Lenosky, J. D. Kress, and L. A. Collins, Phys. Rev. B **56**, 5164 (1997).

[10] L. B. Da Silva *et al.,* Phys. Rev. Lett. **78**, 483 (1997); R. Cauble *et al.,* Phys. Plasmas **4**, 1857 (1997); G. W. Collins *et al.,* Science **281**, 1178 (1998).

[11] Y. B. Zel'dovich and Y. P. Raizer, *Physics of Shock Waves and High-Temperature Hydrodynamic Phenomena* (Academic Press, New York, 1966).

[12] P. M. Celliers *et al.,* Phys. Rev. Lett. **84**, 5564 (2000).

[13] W. J. Nellis, A. C. Mitchell, M. van Theil, G. J. Devine, R. J. Trainor, and N. Brown, J. Chem. Phys. **79**, 1480 (1983).

[14] N. C. Holmes, M. Ross, and W. J. Nellis, Phys. Rev. B **52**, 15 835 (1995); W. J. Nellis, M. Ross, and N. C. Holmes, Science **269**, 1249 (1995).

[15] E. M. Campbell, Laser Part. Beams **9**, 209 (1991).

[16] S. N. Dixit, M. D. Feit, M. D. Perry, and H. T. Powell, Opt. Lett. **21**, 1715 (1996).

[17] A. F. Ioffe and A. R. Regel, Prog. Semicond. **4**, 237 (1960); N. F. Mott, Philos. Mag. **26**, 1015 (1972); Y. T. Lee and R. M. More, Phys. Fluids **27**, 1273–1286 (1984).

[18] G. W. Collins *et al.,* Phys. Plasmas **5**, 1864 (1998).

[19] From the known D_2 photoionization cross section [20], the mean-free path of ionizing photons in unshocked D_2 is <40 nm. For $T \sim 10$ eV, typical of a shocked Al pusher at the highest pressures recorded, the photoionization rate in D_2 is $\sim 5 \times 10^{22}\ \text{cm}^{-3}\,\text{ns}^{-1}$. The fraction of D_2 photoionized in the period (~1 ps) before the shock overtakes the volume is about ~0.5%. This will not effect the steady state 400-nm emission signal.

[20] J. W. Gallagher *et al.,* J. Phys. Chem. Ref. Data **17**, 9 (1988).

[21] S. T. Weir, A. C. Mitchell, and W. J. Nellis, Phys. Rev. Lett. **76**, 1860 (1996); W. J. Nellis *et al.,* Science **273**, 936 (1996).